Applied Catalysis B: Environmental 242 (2019) 389–396

Contents lists available at ScienceDirect

Applied Catalysis B: Environmental

journal homepage: www.elsevier.com/locate/apcatb

# Design of plasmonic CuCo bimetal as a nonsemiconductor photocatalyst for synchronized hydrogen evolution and storage

Piyong Zhang[a], Gongchang Zeng[b], Ting Song[a], Shaobin Huang[b], Tingting Wang[a], Heping Zeng[a,*]

[a] Key Laboratory of Functional Molecular Engineering of Guangdong Province, School of Chemistry and Chemical Engineering, South China University of Technology, Guangzhou, 510641, PR China

[b] School of Environment and Energy, South China University of Technology, Guangzhou, 510641, PR China

ARTICLE INFO

*Keywords:*
CuCo bimetal
Surface plasmon resonance
Photocatalytic water splitting
Hydrogen storage

ABSTRACT

Solar-driven hydrogen evolution with sustainable energy sources, which require earth-abundant, robust and efficient photocatalysts for fuel production, is highly desirable. Here, we propose an alternative promising configuration of a dendrite-like plasmonic CuCo bimetal as a nonsemiconductor photocatalyst, which exhibits exceptional photocatalytic activities for $H_2$ evolution (77.1 μmol $g^{-1}$ $h^{-1}$) under sunlight irradiation without a sacrificial agent. Notably, a certain amount of hydrogen evolved by photocatalytic water splitting was conserved by the photocatalyst at room temperature, demonstrating that the integration of hydrogen evolution and storage was realized in this device. Electrons were produced by the surface plasmon resonance (SPR) effect of the Cu component in CuCo bimetal, and Co nanosheets were grown in situ on the surface of Cu, which can facilitate the transfer of photoinduced charge as a cocatalyst. Specifically, the photocatalyst shows excellent chemical stability with X-ray photoelectron spectroscopy and X-ray diffraction characterization after four consecutive cycles over a total of 20 h. This work provides insights into a plasmonic nonsemiconductor photocatalytic system in the hydrogen energy field.

## 1. Introduction

Recently, plasmonic photocatalysts with a fascinating surface plasmon resonance (SPR) effect have attracted tremendous attention in the field of efficient conversation of solar energy to chemical energy because they can harvest and utilize low-energy photons from sunlight even in the near-infrared region [1–5]. With resonant photon excitation in the incident light, collective oscillations of free charge carriers will occur on the surface of plasmonic photocatalysts and the oscillation electrons can participate in photocatalytic reactions [6–9]. In this regard, one successful paradigm is the introduction of plasmonic noble-metal as a co-catalyst into the photocatalytic system by promoting charge separation and transfer, such as with Au and Ag [10–12]. However, Au and Ag are only cocatalysts and the core of the photocatalytic system is still a semiconductor. Moreover, these noble-metals are expensive and not beneficial for large-scale applications. Plasmonic Cu as a photocatalyst has drawn considerable interest due to its SPR effect, high conductivity, low cost and promising photocatalytic activity, and its photocatalytic properties have been investigated [13,14]. Therefore, Cu is a promising candidate in the photocatalytic field as a nonsemiconductor photocatalyst, which could greatly broaden the scope of the photocatalytic system.

Alloying with other metals to form bimetal is an effective method to change the intrinsic activity of the Cu activity sites. The electron transfer process can be tuned, and the recombination drawback of electron-hole pair can be suppressed due to strain and ligand effects after alloying [15,16]. Cobalt (Co), is a stable, abundant and low-cost metal in the earth and, has broad-spectrum absorption properties and excellent charge transfer abilities [17,18]. More importantly, the hydrogen storage capacity of Co has been reported and this special property can realize the integration of hydrogen evolution and storage [17]. Hence, plasmonic Cu couples with Co to form a bimetal, potentially enabling highly efficient photocatalytic $H_2$ evolution and storage. CuCo bimetal has been applied in many fields such as hydrolytic dehydrogenation of ammonia borane [19], higher alcohol synthesis from syngas [20,21] and syngas conversion [22]. However, to date, the photocatalytic application of plasmonic CuCo bimetal has not been reported.

In this study, a plasmonic CuCo bimetal photocatalyst is rationally designed and prepared using hydrothermal growth. The orientation growth of Co nanosheets grown on the surface of dendrite-like Cu was obtained, and the bimetal activity of the photocatalytic overall water

* Corresponding author.
*E-mail address:* hpzeng@scut.edu.cn (H. Zeng).

https://doi.org/10.1016/j.apcatb.2018.10.020
Received 8 August 2018; Received in revised form 4 October 2018; Accepted 7 October 2018
Available online 09 October 2018

splitting was investigated. Furthermore, the bimetal photocatalyst shows an interesting hydrogen storage response. Two major challenges of hydrogen evolution and storage can be solved simultaneous. This material is a choice for bimetal components because dendrite-like Cu shows an SPR effect for the production of photoinduced electrons, and its work function is lower than that of Co, leading to charge transfer from Cu to Co under a general excitation. Through transient photocurrent responses and steady-state photoluminescence spectra, we demonstrate that SPR excitation of CuCo bimetal can induce the transfer of plasmonic electron from Cu to Co, boosting the production of photoinduced electrons for executing the photocatalytic reaction. In this way, CuCo bimetal prepared with an optimal temperature and ratio exhibits enhanced photocatalytic activity compared with pure dendrite-like Cu under sunlight irradiation.

## 2. Experimental

### 2.1. Materials

All reagents are analytical grade and used without further purification and deionized water was used in all experiments. Cobalt chloride hexahydrate ($CoCl_2{\cdot}6H_2O$) (AR), copper chloride dihydrate ($CuCl_2{\cdot}2H_2O$) (AR), lactic acid (97%) ethylenediamine (AR), sodium hypophosphite (AR), sodium hydrate (NaOH) and absolute ethanol were purchased from Sinopharm Chemical Reagent Co. Ltd., P.R. China.

### 2.2. Synthesis of CuCo bimetal

CuCo bimetal was prepared using the hydrothermal method described below. In a typical synthesis, $x$ mmol of $CuCl_2{\cdot}2H_2O$ and 1-$x$ mmol of $CoCl_2{\cdot}6H_2O$ were dissolved in 60 mL of 2 M NaOH solution, in which $x$ is 1, 0.9, 0.8, 07, 0.6, 0.5 and 0, followed by stirring for 30 min. Subsequently, 1.5 mL of ethylenediamine was dispersed in the mixture and stirred for 10 min, and then 5 mmol of sodium hypophosphite was added to the mixed solution with stirring for 30 min. Next, the mixture was transferred to a Teflon-lined autoclave. The autoclave was sealed and heated to 200 °C within 2 h and kept at this temperature for 15 h, followed by natural cooling to room temperature. CuCo bimetal products with different proportion of Cu were denoted as Cu, Co, $CuCo_{9:1}$, $CuCo_{8:2}$, $CuCo_{7:3}$, $CuCo_{6:4}$, $CuCo_{5:5}$, respectively. In addition, $CuCo_{7:3}$ was also prepared at various temperatures (140, 160, 180, 200 and 220 °C). The CuCo products were collected by centrifugation and washed using three times each with distilled water and absolute ethanol. Finally, the products were dried at 40 °C for 6 h under vacuum. A schematic for the synthetic process of the photocatalyst is shown in Scheme 1. The instruments used for characterization are supplied in the Supporting Information.

### 2.3. Photocatalytic overall water splitting

Photocatalytic activities for overall water splitting were performed under sunlight, and experiments were performed in a Pyrex glass reaction cell with a 300-mL capacity and 7.5-$cm^2$ area connected to a closed gas circulation system. In a typical photocatalytic reaction, 70 mL of deionized water and 5 mg of catalyst were added to the reactor and degassed for approximately 0.5 h before irradiation. A 300 W Xenon lamp (PLS-SXE300CUV, Perfect light. Co. Ltd., Beijing) was used to simulate the solar spectrum as it reaches the earth's surface (AM 1.5 G). The evolved gas was determined using online gas chromatography with a TCD detector (GC-7900, Tianmei, 5 Å molecular sieve column, with argon as the carrier gas). A photograph of the photocatalytic hydrogen production testing system is shown in Fig. S1.

### 2.4. Photoelectrochemical measurements

Electrochemical measurements were conducted on a CHI660C Instruments electrochemical workstation with a standard three-electrode system in 1 M $Na_2SO_4$ solution at room temperature. A modified FTO, a platinum wire, and an Ag/AgCl electrode (3 mol $L^{-1}$ KCl) were used as the working electrode, the counter electrode, and the reference electrode, respectively. The FTO electrode was cleaned by ultrasonication in ethanol, and dried at room temperature. Then, 25 mg of catalyst was suspended in 5 mL of ethyl cellulose/ethanol solution (0.25 wt% ethyl cellulose) to form a homogenous ink under ultrasonication. Then, 10 μL of catalyst ink was dropped onto the FTO glass with a fixed area and was dried using an infrared lamp.

## 3. Results and discussion

### 3.1. Formation and characterization

XRD patterns were used to analyze the crystallization degree and crystal structure of the samples. As shown in Fig. 1a, one can see two different crystalline phases, which are attributed to the cobalt phase (JCPDS NO. 89-4308) [23] and copper phase (JCPDS NO. 04-0836) [24]. The cobalt phase was not formed at 140 °C and only the copper phase was generated due to different standard reduction potentials of Cu and Co [25]. When the temperature was above 140 °C, an apparent cobalt phase appeared in the sample. Notable, the diffraction peaks of Cu at 43.4° and Co at 41.6° were overlapped at 200 °C (marked by green circle), indicating that partial mutual insertion of cobalt and copper atoms occured rather than physical mixing. There was no obvious mutual insertion phenomenon at other temperatures due to the different evolution rate of Cu and Co metals with hydrothermal methods at different temperature, suggesting that a suitable temperature is indispensable for the formation of mutual insertion CuCo bimetal [26]. Furthermore, the peak intensity of the (002) plane was stronger than the (101) plane in Co metal phase, which is opposite the PDF card of Co (JCPDS NO. 89-4308). This phenomenon may be assigned to orientation growth of Co nanosheets and this result can also be found in pure Co nanosheets (Fig. S2). Moreover, the XRD patterns of different ratios of CuCo bimetal were also examined and results are shown in Fig. S3. In addition, no evidence of impurities was observed in the XRD patterns of these catalysts, indicating that the expected crystal compositions of the CuCo bimetal photocatalysts were obtained using the hydrothermal method.

UV-visible diffuse reflectance spectra were recorded in Fig. 1b to investigate the optical behavior of the photocatalysts. Due to the SPR effect of the Cu component, a characteristic SPR absorption peak is observed at a wavelength of 600 nm for CuCo bimetal and pure Cu [27–29]. Co metal shows strong absorption from the ultraviolet to near-infrared field. One important merit of the unique CuCo bimetal is that the Co metal can superimpose light absorption on that of dendrite-like Cu to modulate the optical properties of the CuCo bimetal. As a consequence, the CuCo bimetal generated an enhanced absorption spectrum beyond 600 nm (featured absorption of Co), promoting solar energy absorption and utilization.

The structures and morphologies of the samples were characterized by scanning electron microscopy (SEM), transmission electron microscopy (TEM) and high-resolution TEM (HRTEM). Isolated Co metal presents a nanosheet structure, and the thickness is approximately 10 nm (Fig. 2a, b). A dendrite-like structure of Cu is observed in Fig. 2c, and the length and width were approximately 3 and 2 μm, respectively. This dendrite-like structure is duplicated in smaller dendrite-like structures on each branch at the nanoscale and its surface is smooth. After combination with Co, the as-synthesized CuCo bimetal inherits the same dendrite-like structure of pristine Cu (Fig. 2d, e, f). A rough surface of CuCo bimetal can be found with further observation due to the existence of Co nanosheets, suggesting that conjoined structures formed between Co and Cu. This modification with Co nanosheets gives rise to a large surface area that is beneficial for enhancing photocatalytic activity. Compared with Co nanosheets prepared with single

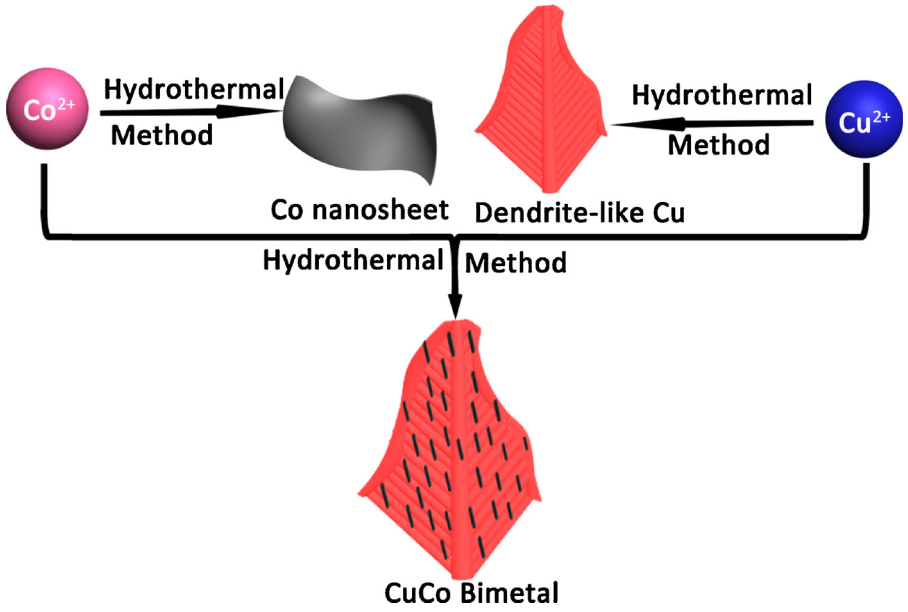


**Scheme 1.** Illustration of the synthetic process.

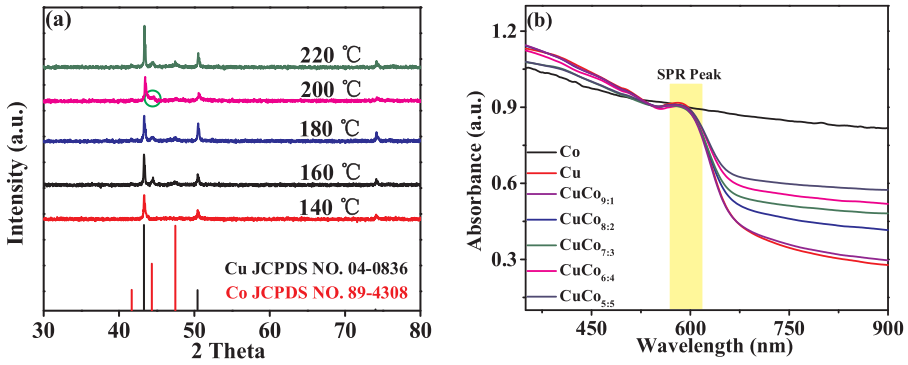


**Fig. 1.** (a) XRD patterns of $CuCo_{7:3}$ prepared at different temperatures and (b) UV–vis diffuse reflectance spectra of different ratios of CuCo bimetal prepared at 200 °C.

$Co^{2+}$, Co nanosheets become smaller in CuCo bimetal, potentially with better activity. The elemental mapping of Cu and Co corresponds well to the profiles of CuCo bimetal in Fig. 2g and energy-dispersive X-ray spectroscopy (EDX) in Fig. 2h further confirms the elemental compositions of Cu and Co in bimetal. Moreover, as confirmed by SEM studies (Fig. 2d, e, f), the CuCo bimetal also exhibits a dendrite-like structure in the TEM image (Fig. 2j). The lattices of CuCo bimetal are visible in HRTEM images (Fig. 2k), revealing the lattice planes of Cu (111) and Co (101) with a characteristic lattice-fringe spacing of 2.09 and 1.91 Å, respectively [30–33]. Moreover, there is a clear demonstration for the mutual insertion of Co and Cu, which are explicitly discerned with a special lattice-fringe spacing of 2.01 Å between the standard cobalt and copper [34]. This mutual insertion phenomenon prevents the detachment of the two metals at the nanoscale, in accordance with the XRD patterns in Fig. 1a.

As shown in Fig. 2e, f, Co nanosheets grown on the surface of dendrite-like Cu could increase their specific surface area. To confirm this assumption, the BET specific surface area ($S_{BET}$) of these samples was performed using adsorption-desorption measurements, and the results are shown in Table S1. Pure Cu shows the least surface area ($12.35\ m^2\ g^{-1}$), while Co nanosheets possess the highest $S_{BET}$ ($36.78\ m^2\ g^{-1}$) among samples. The $S_{BET}$ of CuCo bimetal is larger than pristine Cu after combination with a large special surface area of Co nanosheets, and the values of $S_{BET}$ for CuCo gradually increased with increasing Co nanosheets. More surface active sites can be supplied with the increase in surface area and facilitates charge transfer, improving the photocatalytic activity [35].

The electronic structure and chemical valence of $CuCo_{7:3}$ were investigated by X-ray photoelectron spectroscopy (XPS) in Fig. 3. The survey XPS spectrum exhibits the typical characteristic peaks of Cu, Co, C and O (Fig. 3a), confirming the existence of these elements in the sample. As shown in the Cu 2p spectrum (Fig. 3b), two distinct peaks at 952.3 eV for Cu 2p1/2 and at 932.2 eV for Cu 2p3/2 are attributed to Cu(0) or Cu(I), because their binding energy is similar, and it is difficult to distinguish them in the Cu 2p spectrum [36]. Cu LMM XAEX was performed to further distinguish Cu(0) and Cu(I) in Fig. 3c, confirming that the peak at 918.7 eV is assigned to Cu(0) [37]. This result demonstrated that Cu(II) ions in solution were successfully reduced to Cu (0) using a hydrothermal process. The Co 2p spectra in Fig. 3d show characteristic binding energies of 778.3 and 794.4 eV, assigned to Co 2p3/2 and Co 2p1/2 electrons of Co metal, respectively [38]. This result indicates that the Co nanosheets grown on the Cu outer surface was Co°, in agreement with the XRD patterns. The binding energy at 783.6 and 800.7 eV was matched with shake-up satellites, which were attributed to cobalt oxide [39], likely due to the partial oxidation of the Co nanosheet surface by air during synthesis and storage.

Furthermore, XPS spectral comparisons between monometal and bimetal samples were investigated, and the results are shown in Fig. S4. The slight increase in the Cu 2p spectra in the binding energies of CuCo reveals that some electrons are transferred from Cu to Co in the CuCo

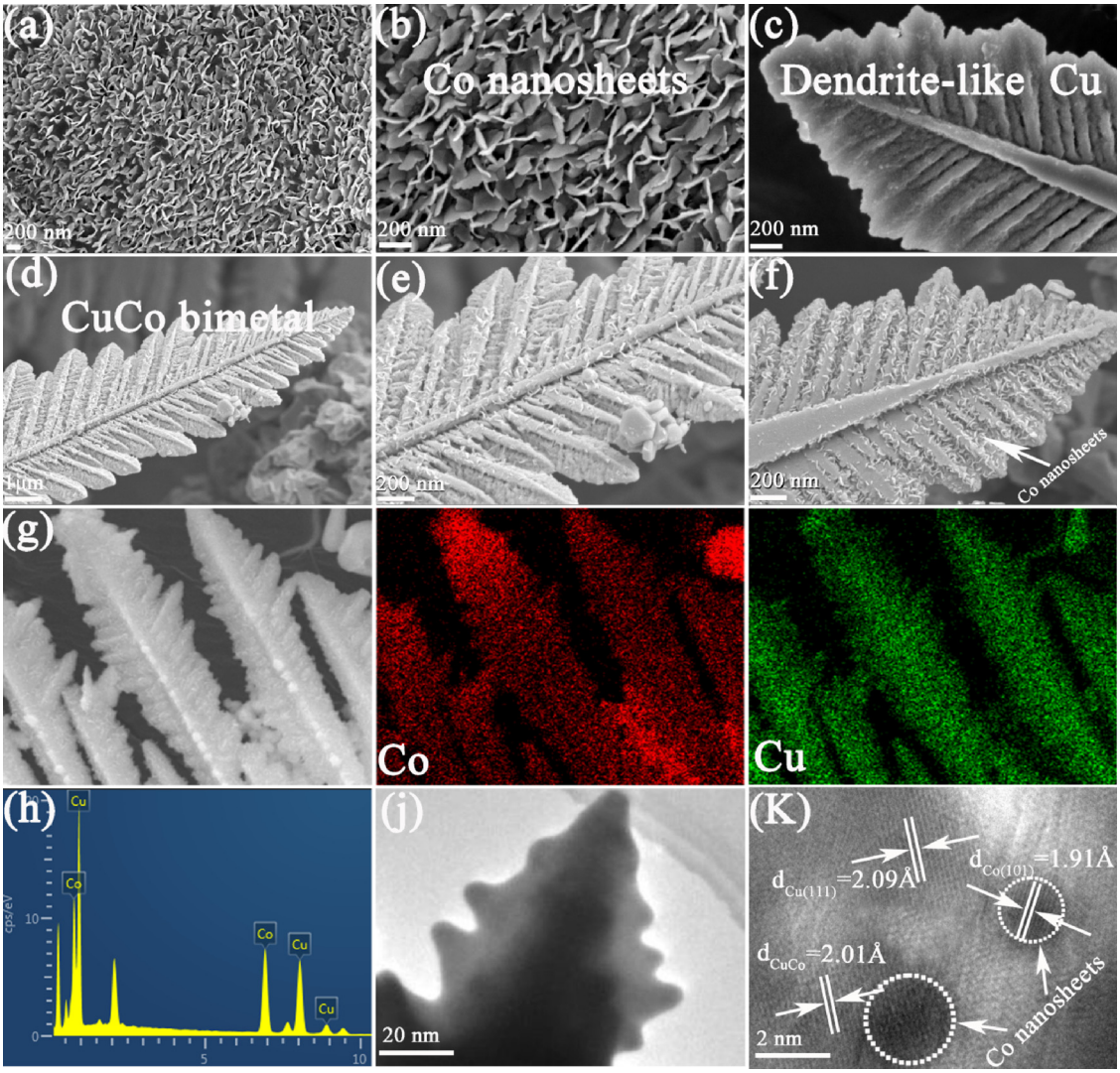


**Fig. 2.** (a), (b) SEM images of Co nanosheets; (c) SEM image of dendrite-like Cu; (d), (e), (f) SEM image of $CuCo_{7:3}$ bimetal; (g) elemental mapping data and (h) EDX spectrum of $CuCo_{7:3}$ bimetal; (j) TEM and (k) HRTEM of $CuCo_{7:3}$ bimetal. All samples were prepared at 200 °C.

bimetal, and there is a possible interaction of Cu with Co [40]. The Co 2p peaks of the CuCo bimetal shift to lower binding energy compared to that of monometal Co, confirming the possible interaction of Cu and Co [41]. Therefore, a strong electron interaction between Cu and Co occurs on the catalyst surface, in which electrons transfer from Cu species to Co species in the bimetal catalyst.

### 3.2. Evaluation of photocatalytic activities

The photocatalytic overall water splitting activities of photocatalysts are investigated under sunlight irradiation without sacrificial reagent. The controlled experiments suggested that no photocatalytic activity was detected in the absence of photocatalyst or without irradiation, indicating that the evolution of $H_2$ and $O_2$ was triggered by a photocatalytic process. As expected, the hydrogen evolution rate of $CuCo_{7:3}$ was lower in the first four hours due to storage in cobalt nanosheets (Fig. 4a). Based on the hydrogen evolution under normal conditions, the $H_2$ storage capacity of CuCo photocatalyst was 0.42 wt %. After four hours, the hydrogen evolution rate becomes constant. Fig. 4b shows the $H_2$ evolution rate of CuCo bimetal with different ratios from photocatalytic overall water splitting, and these data were collected after irradiation for four hours. Pure Co nanosheets have no photocatalytic activity, and dendrite-like Cu exhibits obvious photocatalytic $H_2$ evolution with a rate of 21.9 μmol $g^{-1}$ $h^{-1}$ due to the SPR effect. All CuCo bimetal photocatalysts showed a higher photocatalytic $H_2$ evolution rate than the dendrite-like Cu itself, and the CuCo bimetal with an optimal proportion of 7:3 showed the highest photocatalytic $H_2$ evolution rate (77.1 μmol $g^{-1}$ $h^{-1}$). This result demonstrated that Co nanosheets, as cocatalysts, play an important role in the enhancement of photocatalytic activity. The photocatalytic activity was gradually improved after alloying with Co nanosheets, and then decreased with a further increase in the molar ratio to $CuCo_{5:5}$. Due to the excessive Co nanosheets covering the Cu photoactive sites, light was shielded, resulting in a low production of photoexcited charge carriers. Although cobalt oxide was detected on the surface of Co nanosheets using XPS spectra, the pure Co nanosheets sample showed no water splitting activity, indicating that cobalt oxide has no photocatalytic activity for water splitting in this condition. In addition, the photocatalytic $H_2$ evolution rates of samples were also investigated in the presence of lactic acid sacrificial agents, and the results are shown in Fig. S5.

The photocatalytic stability of $CuCo_{7:3}$ prepared at 200 °C were conducted via four successive runs without renewing the photocatalyst, and each run lasted 5 h. As shown in Fig. 4c, the $CuCo_{7:3}$ bimetal sample showed high stability during the repeating photocatalytic reaction, and $H_2$ and $O_2$ evolution rates were stable after 20 h. The X-ray diffraction

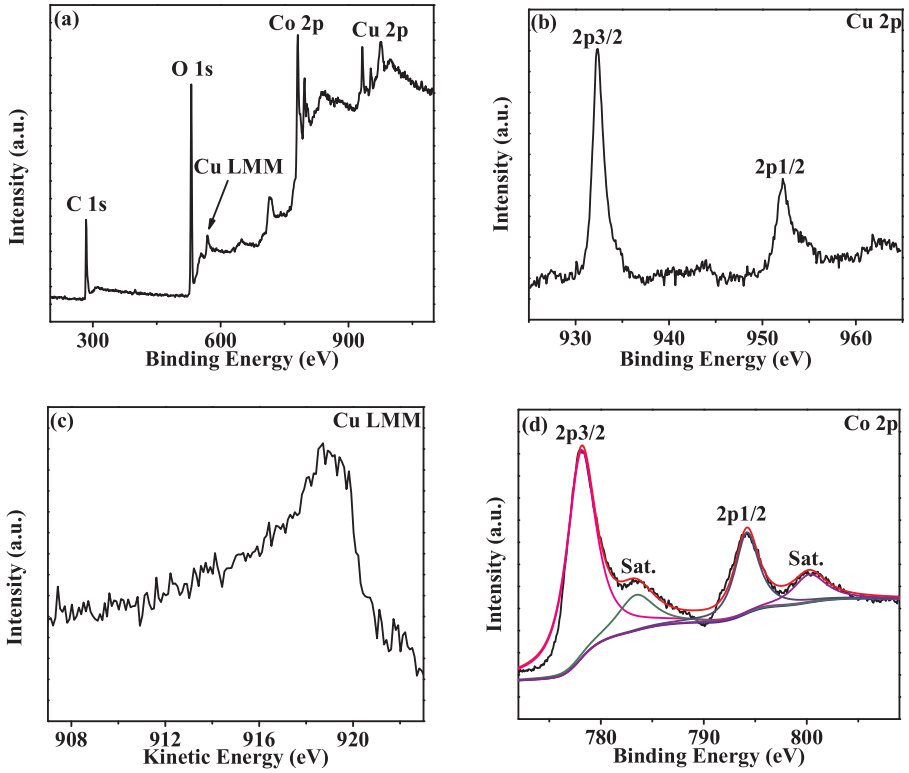


**Fig. 3.** XPS spectra of $CuCo_{7:3}$ prepared at 200 °C, (a) survey spectrum, (b) Cu 2p narrow scan, (c) Cu LMM narrow scan, (d) Co 2p narrow scan.

patterns (Fig. S4) of the $CuCo_{7:3}$ bimetal were performed after the recycle test, and no apparent changes were observed in the examinations, suggesting that $CuCo_{7:3}$ bimetal had excellent chemical stability during the photocatalytic reaction. Furthermore, XPS spectra were also investigated after the recycle test, as shown in Fig. S6. Similar spectra were observed for Cu 2p and Co 2p before and after the recycle test, further confirming chemical stability under long time irradiation. It is worth noting that signals of Co 2p show a significant shift (approximately 2 eV) after the photocatalytic reaction, due to an interaction between Co and H [42,43], demonstrating hydrogen storage on the Co

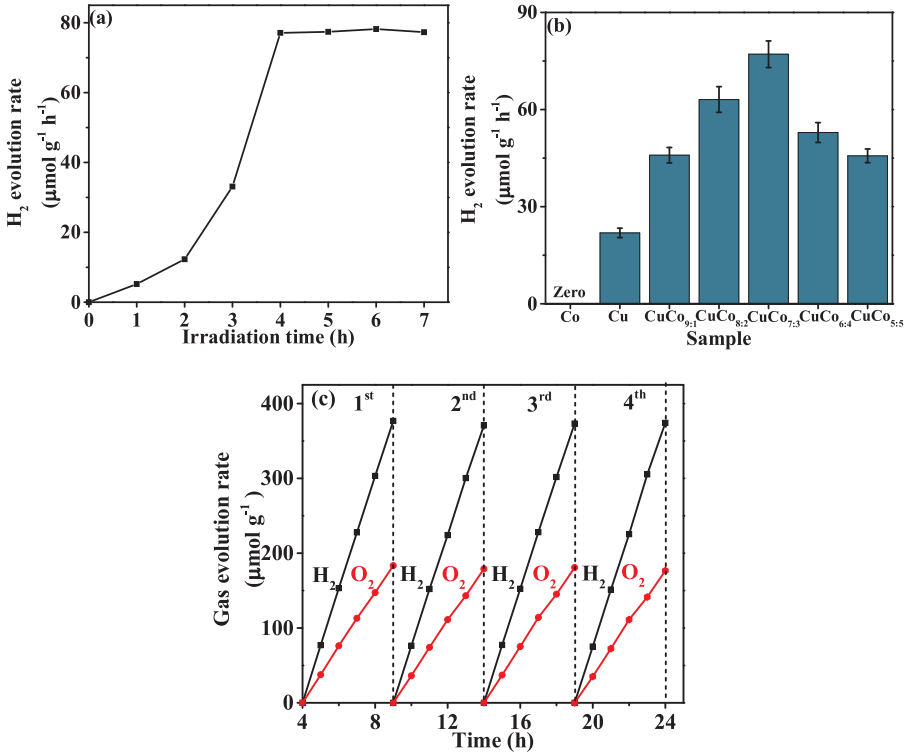


**Fig. 4.** Photocatalytic activity of samples prepared at 200 °C, (a) photocatalytic water splitting of $CuCo_{7:3}$ for $H_2$ evolution in the 7 h, (b) $H_2$ evolution of CuCo bimetal with different ratios from photocatalytic overall water splitting, and (c) recycling test of $CuCo_{7:3}$ for water splitting.

nanosheets. In addition, $H_2$ evolution rates from the photocatalytic overall water splitting of $CuCo_{7:3}$ bimetal prepared at different temperatures were also performed, and the results are shown in Fig. S7. The $CuCo_{7:3}$ bimetal prepared at 200 °C possessed the highest $H_2$ evolution rate, approximately two fold higher than that of the $CuCo_{7:3}$ bimetal prepared at 160 °C A suitable temperature allows the Co nanosheets to effectively contact the Cu, and the presence of partial mutual insertion of cobalt and copper atoms is demonstrated in Figs. 1a and 2 k. Moreover,a larger work function of Co metal compared to Cu makes charge transfer thermodynamically favorable from the dendrite-like Cu to the Co nanosheets. Effective contact and exact charge direction would promote the separation and transfer of the plasmonic electron, enhancing photocatalytic separation. An unsuitable temperature cannot form effective contact between two phases.

Temperature programmed desorption (TPD) analysis of the catalyst was conducted after photocatalytic water splitting to further demonstrate that hydrogen evolved in the photocatalytic reaction has been stored in the Co metal, as shown in Fig. S8. Gas desorption peaks are observed in three temperature zones: one at 140–200 °C due to the CuCo interface site [18], one at 238 °C assigned to $H_2$ desorption from a stepped Co surface [44], and one at 332 °C attributed to $H_2$ desorption from the Co terrace [45]. These peaks confirm that hydrogen was released from the CuCo bimetal after 332 °C, demonstrating that hydrogen was stored in the photocatalyst. According to a previous report [46], hydrogen could be released from Co metal-based materials at temperatures ranging from 77 to 600 °C (which includes 332 °C).

The photocatalytic activity of CuCo bimetal has been investigated under sunlight irradiation; however, some inevitable oxides, as a semiconductor photocatalyst, could also contribute to photocatalysis under sunlight irradiation. To eliminate this interference and demonstrate that photocatalysis derives from an SPR effect, wavelengths within the SPR frequencies of light irradiation were used for photocatalysis. Monochromatic light irradiation at a wavelength of $600 \pm 10$ nm was obtained with a bandpass filter; other experimental conditions were unchanged. Plasmon resonance can be induced at this wavelength, and the semiconductor showed little response. $CuCo_{7:3}$ shows a decay in the $H_2$ evolution rate with 10 μmol $g^{-1}$ $h^{-1}$ due to the decrease in total photon flux available for photocatalytic water splitting. This result demonstrates that photocatalytic water splitting was driven by the SPR effect.

### 3.3. Discussion on mechanism

The CuCo bimetal was examined in light of the photoelectrochemical to corroborate the ability of the SPR-initiated photoexcited charge to transfer solar energy to hydrogen. The typical photocurrent-time response of the metal photoelectrode was investigated (Fig. 5a), and the spectra display intriguing behavior. When the light was turned on, the photocurrents showed an initial shoot, followed by a steady increase, mimicking the rectangular signal that is expected in a desired case, demonstrating that the carrier was generated under light irradiation. $CuCo_{7:3}$ achieves the highest photocurrent value, in other words the optimum efficiency of electron-hole separation [47,48]. Compared with pure Cu, all CuCo bimetal photocatalysts show higher photocurrent values, consistent with photocatalytic water splitting activity. This phenomenon further confirms that Co nanosheets are excellent cocatalysts that significantly mitigate recombination of the antipodal charge carriers.

To gain further insight into the separation and recombination of plasmon-induced electron-hole pair, the PL spectra were also collected, and the results are shown in Fig. 5b. After modification with Co nanosheets, the PL intensity of the CuCo bimetal was diminished compared to the pure Cu, due to the shuttling or trapping of the plasmon-induced electrons to Co nanosheets, thus retarding the recombination of the electron-hole pair. Furthermore, the electrochemical reduction experiments on the photocatalysts were also investigated in the $N_2$bubbled system, as shown in Fig. 5c. The current in the samples increased with the forward bias voltage, and the cathodic current is attributed to the electrochemical $H_2$ evolution. Compared with pure Cu, much more favorable electrochemical $H_2$ evolution on the CuCo bimetal was obtained, indicating that CuCo bimetal possesses a lower overpotential [49,50]. This result demonstrated that CuCo bimetal is obviously favored thermodynamically to possess better photocatalytic activity.

Based on the above results and discussion, a possible mechanism schematic of the separation and transfer of plasmon-induced electrons in the synthesized CuCo bimetal and the induced photochemical processes is illustrated in Fig. 6. Under sunlight illumination, a resonant collective oscillation occurs between resonant photons and free charge and then decays into the electron-hole pair via Landau Damping [13,51–53]. In the next moment, the plasmon-induced energetic electrons accumulated on the plasmonic Cu, became the charge carriers and were then transferred to Co nanosheets due to a larger work function. Co nanosheets play an important role in retarding the recombination of electron-hole pairs and this view is strongly supported by transient photocurrent responses and PL spectra in Fig. 5. In general, Co nanosheets serve as an electron relay to facilitate the extraction. Afterwards, these charges on the surface of Co nanosheets are directly injected to adsorbed water molecules for water reduction to $H_2$ evolution [54]. Meanwhile, the photogenerated hole on the Cu is scavenged by surrounding water molecules to generate $O_2$.

For water splitting, the photocatalytic activity of CuCo bimetal remarkably outperforms a photocatalyst without Co nanosheets. The improvement stems mostly from the synergistic effect between Cu and Co. (I) Effective interfacial contacts was formed between these two metals, as demonstrated by mutual insertion phenomenon in XRD patterns. Effective interfacial contact is a necessary condition for electron transfer, boosting electron collection. (II) Co (5 eV) possesses a larger work function than Cu (4.65 eV), making charge transfer thermodynamically favorable from the dendrite-like Cu to the Co nanosheets. Taken together, the results demonstrate that plasmonic CuCo bimetal holds great promise as an important design for widespread photocatalytic devices for water splitting involving the use of SPR frequencies photons.

## 4. Conclusions

In summary, dendrite-like plasmonic Cu with photocatalytic activity for $H_2$ evolution was successfully prepared. The collected SPR frequency photons are exclusively transferred to charge carriers via the SPR effect to participate in photocatalytic water splitting. Intriguingly, its photocatalysis could be greatly enhanced after modification with Co nanosheets, especially with an optimal ratio, and even with a respective $\approx$ 3.5-fold time improvement for $H_2$ evolution compared to the Cu itself. Furthermore, it is demonstrated that the exceptional photocatalytic activity is comprehensively ascribed to the cocatalysis effect of Co nanosheets, and greatly promoted charge separation and transfer. More importantly, our newly developed photocatalysts showed an outstanding performance in hydrogen evolution-storage integration at room temperature, which is a desirable property in the photocatalytic hydrogen evolution field. This work provides a plasmonic non-semiconductor photocatalyst for highly effective solar fuel production and storage.

## Acknowledgements

We thank the National Natural Science Foundation of China (No. 21571064, 21371060), the PhDStart-up Fund of Natural Science Foundation of Guangdong Province, the Fundamental Research Funds for the Central Universities and the research fund of the Key Laboratory of Fuel Cell Technology of Guangdong Province for financial support.

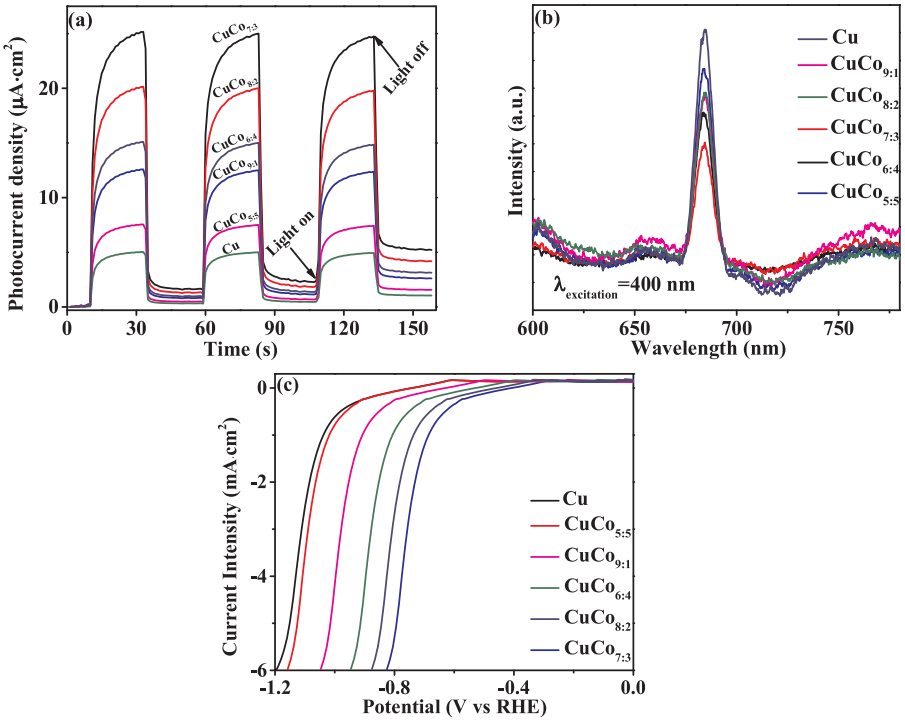


**Fig. 5.** (a) Transient photocurrent responses, (b) photoluminescence (PL) spectra and (c) linear-sweep voltammograms collected with a scan rate of 5 mV/s.

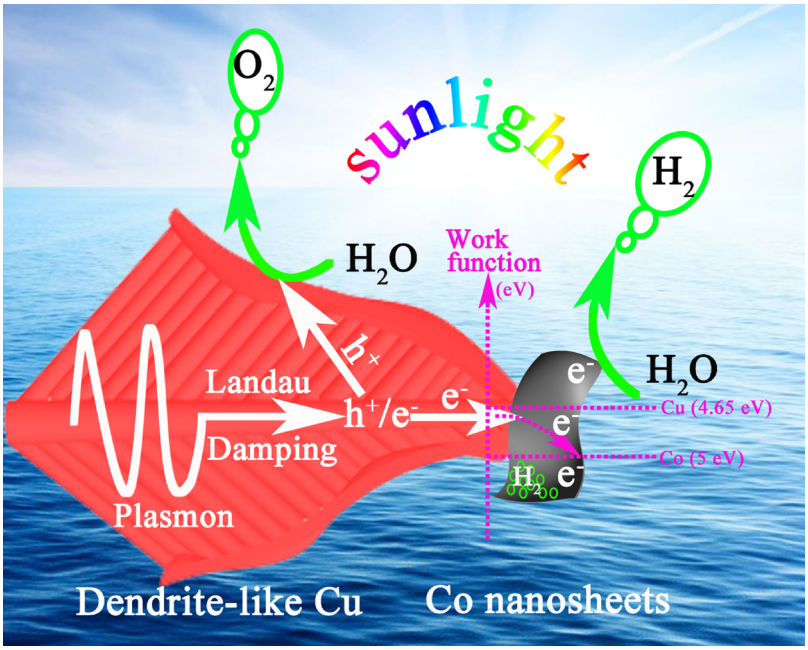


**Fig. 6.** Schematic of plasmon-induced charge separation and transfer on CuCo bimetal.

## Appendix A. Supplementary data

Supplementary material related to this article can be found, in the online version, at doi:https://doi.org/10.1016/j.apcatb.2018.10.020.

## References

[1] N. Zhang, C. Han, Y. Xu, J.J. Foley IV, D. Zhang, J. Codrington, S.K. Gray, Y. Sun, Nat. Photonics 10 (2016) 473–482.
[2] S. Linic, P. Christopher, D.B. Ingram, Nat. Mater. 10 (2011) 911–921.
[3] A. Giugni, B. Torre, A. Toma, M. Francardi, M. Malerba, A. Alabastri, R.P. Zaccaria, M.I. Stockman, E.D. Fabrizio, Nat. Nanotechnol. 8 (2013) 845–852.
[4] P. Zhang, T. Song, T. Wang, H. Zeng, Appl. Catal. B: Environ. 225 (2018) 172–179.
[5] Y. Zhang, S.J. Park, J. Catal. 355 (2017) 1–10.
[6] G.V. Hartland, Chem. Rev. 111 (2011) 3858–3887.
[7] J. Olson, S. Dominguez-Medina, A. Hoggard, L. Wang, W. Chang, S. Link, Chem. Soc. Rev. 44 (2015) 40–57.
[8] D.Y. Wan, et al., Nat. Commun. 8 (2017) 15070.
[9] Y. Zhang, S.J. Park, J. Catal. 361 (2018) 238–247.
[10] Y. Shi, J. Wang, C. Wang, T. Zhai, W. Bao, J. Xu, X. Xia, H. Chen, J. Am. Chem. Soc. 137 (2015) 7365–7370.
[11] G. Liu, P. Li, G. Zhao, X. Wang, J. Kong, H. Liu, H. Zhang, K. Chang, X. Meng, T. Kako, J. Am. Chem. Soc. 138 (2016) 9128–9136.
[12] Y. Kang, Y. Gong, Z. Hu, Z. Li, Z. Qiu, X. Zhu, P.M. Ajayan, Z. Fang, Nanoscale 7 (2015) 4482–4488.
[13] J. Li, S.K. Cushing, F. Meng, T.R. Senty, A.D. Bristow, N. Wu, Nat. Photonics 9 (2015) 601–607.
[14] P. Zhang, T. Song, T. Wang, H. Zeng, Appl. Catal. B: Environ. 206 (2017) 328–335.

[15] A. Yousef, M. Akhtar, N. Barakat, M. Motlak, O. Yang, H. Kim, Electrochim. Acta 102 (2013) 142–148.
[16] S. Zhang, L. Nguyen, J.X. Liang, J. Shan, J. Liu, A.I. Frenkel, A. Patlolla, W. Huang, J. Li, F. Tao, Nat. Commun. 6 (2015) 7938.
[17] Y. Yang, P. Gao, Y. Wang, L. Sha, X. Ren, J. Zhang, P. Yang, T. Wu, Y. Chen, X. Li, J. Mater. Chem. A 5 (2017) 9198–9203.
[18] E.A. Lewis, M.D. Marcinkowski, C.J. Murphy, M.L. Liriano, E.C.H. Sykes, J. Phys. Chem. Lett. 5 (2014) 3380–3385.
[19] Y. Liu, J. Zhang, H. Guan, Y. Zhao, J. Yang, B. Zhang, Appl. Surf. Sci. 427 (2018) 106–113.
[20] G. Liu, T. Niu, D. Pan, F. Liu, Y. Liu, Appl. Catal., A 483 (2014) 10–18.
[21] W. Gao, Y. Zhao, H. Chen, H. Chen, Y. Li, S. He, Y. Zhang, M. Wei, D.G. Evans, X. Duan, Green Chem. 17 (2015) 1525–1534.
[22] R. Ba, Y. Zhao, L. Yu, J. Song, S. Huang, L. Zhong, Y. Sun, Y. Zhu, Nanoscale 7 (2015) 12365–12371.
[23] S. Gao, Y. Lin, X. Jiao, Y. Sun, Q. Luo, W. Zhang, D. Li, J. Yang, Y. Xie, Nature 529 (2016) 68–71.
[24] H. Liu, T. Wang, H. Zeng, Part. Part. Syst. Char. 32 (2015) 869–873.
[25] S. Zhang, H. Zeng, Chem. Mater. 22 (2010) 1282–1284.
[26] B. Zhang, W. Zhao, G. Shao, B. Fan, R. Zhang, ACS Appl. Mater. Interfaces 7 (2015) 12951–12960.
[27] M. Lin, G. Kim, J. Kim, J. Oh, J. Nam, J. Am. Chem. Soc. 139 (2017) 10180–10183.
[28] G.H. Chan, J. Zhao, E.M. Hicks, G.C. Schatz, R.P. Van Duyne, Nano Lett. 7 (2007) 1947–1952.
[29] T. Togashi, M. Nakayama, A. Hashimoto, M. Ishizaki, K. Kanaizuka, M. Kurihara, Dalton Trans. 47 (2018) 5342–5347.
[30] L. He, C. Liu, J. Hu, W. Gu, Y. Zhang, L. Dong, X. Fu, J. Tang, CrystEngComm 18 (2016) 7764–7771.
[31] M.B. Gawande, A. Goswami, F.X. Felpin, T. Asefa, X. Huang, R. Silva, X. Zou, R. Zboril, R.S. Varma, Chem. Rev. 116 (2016) 3722–3811.
[32] Y. Niu, X. Huang, L. Zhao, W. Hu, C. Li, ACS Sustain. Chem. Eng. 6 (2018) 3556–3564.
[33] P. Wang, Z. Zhang, X. Yan, M. Xu, Y. Chen, J. Li, J. Li, K. Zhang, Y. Lai, J. Mater. Chem. A 6 (2018) 14178–14187.
[34] A. Cao, G. Liu, Y. Yue, L. Zhang, Y. Liu, RSC Adv. 5 (2015) 58804–58812.
[35] M. Waki, Y. Maegawa, K. Hara, Y. Goto, S. Shirai, Y. Yamada, N. Mizoshita, T. Tani, W.J. Chun, S. Muratsugu, M. Tada, A. Fukuoka, S. Inagaki, J. Am. Chem. Soc. 136 (2014) 4003–4011.
[36] L. Chiang, R. Doong, J. Hazard. Mater. 277 (2014) 84–92.
[37] P. Zhang, T. Wang, H. Zeng, Appl. Surf. Sci. 391 (2017) 404–414.
[38] X. Chen, K. Shen, J. Chen, B. Huang, D. Ding, L. Zhang, Y. Li, Chem. Eng. J. 330 (2017) 736–745.
[39] H. Chen, K. Shen, Q. Mao, J. Chen, Y. Li, ACS Catal. 8 (2018) 1417–1428.
[40] A. Bulut, M. Yurderi, I.E. Ertas, M. Celebi, M. Kaya, M. Zahmakiran, Appl. Catal. B 180 (2016) 121–129.
[41] Y. Liu, J. Zhang, H. Guan, Y. Zhao, J. Yang, B. Zhang, Appl. Surf. Sci. 427 (2018) 106–113.
[42] D. Bao, P. Gao, C. Li, G. Wu, Y. Wang, Y. Chen, H. Zhou, P. Yang, Eur. J. Inorg. Chem. 21 (2016) 3371–3375.
[43] H.B. Dai, Y. Liang, P. Wang, Catal. Today 170 (2011) 27–32.
[44] P. van Helden, J.A. van den Berg, C.J. Westrate, ACS Catal. 2 (2012) 1097–1107.
[45] L. Xu, Y. Ma, Y. Zhang, B. Chen, Z. Wu, Z. Jiang, W. Huang, J. Phys. Chem. C 115 (2011) 3416–3424.
[46] Z.Y. Zhong, Z.T. Xiong, L.F. Sun, J.Z. Luo, P. Chen, X. Wu, J. Lin, K.L. Tan, J. Phys. Chem. B 106 (2002) 9507–9513.
[47] T. Song, P. Zhang, T. Wang, A. Ali, H. Zeng, Appl. Catal., B 224 (2018) 877–885.
[48] Y. Zhang, S.J. Park, Appl. Catal., B 240 (2019) 92–101.
[49] Y. Li, D. Gao, S. Peng, G. Lu, S. Li, Int. J. Hydrogen Energy 36 (2011) 4291–4297.
[50] Y. Xin, X. Kan, L. Gan, Z. Zhang, ACS Nano 11 (2017) 10303–10312.
[51] H. Petek, S. Ogawa, Prog. Surf. Sci. 56 (1997) 239–310.
[52] C. Clavero, Nat. Photonics 8 (2014) 95–103.
[53] T. Tatsuma, H. Nishi, T. Ishida, Chem. Sci. 8 (2017) 3325–3337.
[54] M.J. Kale, T. Avanesian, P. Christopher, ACS Catal. 4 (2014) 116–128.

# Update


## Applied Catalysis B: Environmental

**Volume 290, Issue , 5 August 2021, Page**

**DOI: https://doi.org/10.1016/j.apcatb.2020.119772**

Applied Catalysis B: Environmental 290 (2021) 119772

Contents lists available at ScienceDirect

Applied Catalysis B: Environmental

journal homepage: www.elsevier.com/locate/apcatb

Corrigendum

# Corrigendum to "Design of plasmonic CuCo bimetal as a nonsemiconductor photocatalyst for synchronized hydrogen evolution and storage" [Appl. Catal. B: Environ. 242 (2019) 389–396 APCATB 17108]

Piyong Zhang [a], Gongchang Zeng [b], Ting Song [a], Shaobin Huang [b], Tingting Wang [a], Heping Zeng [a,c,*]

[a] Key Laboratory of Functional Molecular Engineering of Guangdong Province, School of Chemistry and Chemical Engineering, South China University of Technology, Guangzhou, 510641, PR China
[b] School of Environment and Energy, South China University of Technology, Guangzhou, 510641, PR China
[c] School of Chemistry, South China Normal University, Guangzhou, 510006, PR China

The authors regret the additional affiliation/contact information of the corresponding author Professor Heping Zeng. The additional affiliation/contact information of the corresponding author Professor Heping Zeng is :

School of Chemistry, South China Normal University, Guangzhou,510006, PR China.

The authors would like to apologise for any inconvenience caused.

DOI of original article: https://doi.org/10.1016/j.apcatb.2018.10.020.
* Corresponding author at: School of Chemistry, South China Normal University, Guangzhou, 510006, PR China.
*E-mail addresses:* zenghp@scnu.edu.cn, hpzeng@scut.edu.cn (H. Zeng).

https://doi.org/10.1016/j.apcatb.2020.119772

Available online 16 December 2020